A Site-Specific LoRaWAN Parameters Selection Approach with Multi-loss Propagation Model

Shubham Pandey[1], Preti Kumari[1], Hari Prabhat Gupta[1,2], Devashish Rai[1], and S. V. Rao[3]
[1]Dept. of CSE, IIT(BHU) Varanasi, INDIA, [2]Embryocraft Sol. Pvt. ltd., [3]Dept. of CSE, IIT Guwahati, INDIA
{shubhampandey.rs.cse21, pretikri.rs.cse17, hariprabhat.cse, devashish.rai.cse20}@iitbhu.ac.in, svrao@iitg.ernet.in

***Abstract*—Long Range Wide Area Network (LoRaWAN) emerges as a promising solution due to its impressive communication range. However, achieving this range in real-world environments is influenced by signal absorption and reflection caused by obstructions such as buildings, vegetation, and the ground along the path to the gateway. This challenge is amplified in unknown sites where infrastructure details are unavailable before the deployment of LoRaWAN. To address the aforementioned challenges, the paper proposes an approach to determine and configure the LoRaWAN parameters for a given site. The approach introduces a method that automatically detects obstructions solely using site images, thereby eliminating the need for manual intervention. Subsequently, by employing the concept of a multi-loss propagation model, the approach estimates path loss, taking into account the identified site obstructions along the communication path. Finally, the estimated path loss is utilized to determine site-specific optimal LoRaWAN parameters, aiming to streamline the deployment process and enhance network efficiency. Through extensive experimentation and evaluation in a real-world LoRaWAN deployment, the approach demonstrates significant improvements in communication efficiency and overall network performance.**

***Index Terms*—Communication efficiency, Link quality, LoRaWAN, Signal propagation model**

I. Introduction

Long Range Wide Area Network (LoRaWAN) is an open specification for a Low Power WAN protocol based on Long-Range (LoRa) technology. It emerges as a promising solution due to its extensive communication range, enabling gateways to receive data from nodes in large deployment sites. LoRa technology operates on various network parameters, including Spreading Factors (SFs) ranging from 7 to 12. A low SF provides a higher data rate with lower sensitivity levels at the receiver than a high SF [1]. Transmission Power (TxPower) is another parameter that impacts network performance by influencing both the range of communication and energy consumption. The receiving power at the nodes significantly determines the feasibility of the communication link.

The LoRaWAN communication range is contingent upon various factors, such as deployment site scenarios, locations of senders and receivers, and types of application data [2]. To illustrate the impact of these factors on the communication range, we conducted an experimental study on the campus site, as discussed in Section III. The study found signals reaching 0.7km on SF10 amidst obstacles, compared to 2km in open space. The limited communication range is due to signal absorption and reflection by various obstructions.

Traditional node deployment, relying on imprecise estimations and expert guesswork, often leads to challenges like weak signals, unstable connections, and data losses. These methods complicate network planning, especially in unfamiliar sites with limited infrastructure details. By introducing an approach that analyzes path loss, SF, transmission, and receiving power while considering environmental obstructions, deployment processes can be streamlined.

Exploring path loss estimation in LoRaWAN deployment highlights challenges in identifying site obstructions. Potential methods like analyzing satellite images or relying on comprehensive site information have limitations; satellite images may lack structural details, complicating obstruction identification. For instance, a low-height building may not obstruct communication between the sender and receiver located in high-rise buildings. This emphasizes the necessity for an efficient solution to accurately determine comprehensive structural information, such as the height of buildings, at the specific site. Moving forward, optimizing LoRaWAN parameters, including SF, TxPower, and received power, is equally crucial for successful LoRaWAN communication.

The current mechanism [3], [4] has predominantly focused on known sites. However, in an unknown site, it often necessitates manual visits to deploy nodes and adjust network parameters by transmitting sample packets [5], [6]. This method is both time-consuming and resource-inefficient. Furthermore, previous studies [4], [7], [8] have primarily emphasized the allocation of network parameters for static nodes, making them inadequate for addressing the distinct requirements of mobile nodes. A novel solution is required to streamline the setting of network parameters in advance, catering to both static and mobile nodes in unfamiliar environments.

This paper presents an approach for determining optimal LoRaWAN parameters for a given site, including SF and TxPower. The approach relies on minimal information about the site, such as standard two-dimensional images of the site and the positions of LoRa transmitters and receivers. It eliminates the need for manual intervention. Specifically, we formulate and solve the following problem in the paper: *How to determine and configure the site-specific optimal LoRaWAN parameters to streamline the deployment process and enhance the efficiency of the network?* To address the problem, we present a **M**ulti-loss **P**ropagation model-based site-specific **LoRa**WAN parameter selection approach, abbreviated as MPLoRa. This approach determines optimal LoRaWAN parameters by leveraging estimated path loss derived from the multi-loss propagation model.

Contributions: To the best of our knowledge, this is the first work to determine the optimal LoRaWAN parameters for a given site with limited information. The major contributions are:

• *Multi-loss propagation model:* The MPLoRa first presents a multi-loss propagation model for LoRa signals in a given site. We conducted an experimental study on the campus site and

ISBN 978-3-903176-63-8 © 2024 IFIP
978-3-903176-63-8/24/$31.00 ©2024 IEEE

created a dataset for the model [9]. This model estimates the path loss between sender and receiver, considering free space, terrain, multi-wall and floor loss, as well as the shadowing effects of surroundings in the network.

• *Identifying communication path obstructions:* To accurately estimate path loss, it is crucial to identify obstructions along the communication path. MPLoRa introduces a method that detects these obstructions using site images and eliminates the need for manual intervention.

• *LoRaWAN network parameters optimization:* Using the obstruction information and the estimated path loss, MPLoRa determines the site-specific optimal LoRaWAN network parameters, including SF and TxPower.

• Finally, we verify the effectiveness of MPLoRa through extensive real-world experiments conducted on a campus site. During the evaluation, we take into account factors such as the mobility of nodes, changes in campus infrastructure, and variations in weather conditions.

The paper is organized as follows. Next section summarizes the background and motivation of work. Section III and Section IV illustrate the deployment scenarios and the design of MPLoRa, respectively. The performance evaluation and conclusions are presented in Section V and Section VI.

II. Related Work and Preliminaries

This section discusses the existing literature and the motivation behind this work. Furthermore, it provides an overview of the various path loss models.

A. Related work

Prior studies have focused on deploying LoRa networks and optimizing parameters [4], [7], [8]. The authors in [7] introduced an Adaptive Data Rate (ADR) algorithm, which facilitates the network server to dynamically adjust the SF and TxPower of the LoRa end devices. In doing so, they encompassed the Signal- to-Noise Ratio of the received signal. Similarly, Liando et al. in [4] conducted large-scale real-world experiments to determine the impact of both line-of-sight and non-line-of-sight conditions on the performance of the LoRa networks. Identifying a notable compromise in performance, they introduced an algorithm tailored for non-line-of-sight scenarios. This algorithm aims to determine the optimal SF and TxPower, accounting for communication distance and node lifetime constraints. Considering the importance of the optimal allocation of SF and TxPower in LoRa networks, the authors in [8] proposed an approach to enhance the throughput and fairness and minimize energy consumption. They considered the effects of imperfect SF orthogonality and co-SF/inter-SF interference.

The authors in [5], investigated ADR mechanisms to configure the communication parameters of LoRa networks in dense IoT scenarios. Extensive simulations revealed a significant impact on ADR performance due to a highly-varying wireless channel. Consequently, they introduced an enhanced version of the original ADR mechanism designed to adapt to variable channel conditions. The study demonstrated that further performance improvements could be achieved by configuring ADR based on the global knowledge of the network. The authors in [3], introduced a LoRa signal propagation model called FLog tailored for orchards. Leveraging orchards' uniform tree shapes and spatial arrangement, FLog employs a 3D model to map wireless signal paths between sensors and gateways. Renzo *et al.* in [6], use lightweight reinforcement learning techniques, namely multi-armed bandits, for each node to select an appropriate SF, based on preferences regarding the trade-off between transmission performance and energy conservation. Further, the authors in [10] addressed the joint optimization problem of channel assignment and Txpower allocation to ensure throughput fairness among users in the LoRa networks.

Limitations in existing work: Current research [3], [4] has predominantly focused on well-known sites. However, in unknown sites, adjusting parameters often requires manual visits and transmission of sample packets [5], [6]. Such methods are both time-consuming and resource-inefficient. Additionally, previous studies [4], [7], [8], [10] often tailor network parameter allocation strategies to static LoRa nodes, overlooking the unique requirements of mobile nodes. This oversight can compromise the adaptability and performance of the system.

B. Motivation of this work

We conducted an experiment to assess the signal quality of LoRa links within a campus site, focusing on the Received Signal Strength Indicator (RSSI) as a key metric. As shown in Fig. 1(a), the receiver is fixed at location C at a height of 30 feet. We consider two senders: one at location A and other at location B, both maintaining a ground-to-ground distance of 650 meters from receiver. To measure the impact on signal strength, both senders are placed first at 5 feet and then at 15 feet height. Both senders are configured to transmit packets using SF = 10 and TxPower = 18dBm. Fig. 1(b) indicates

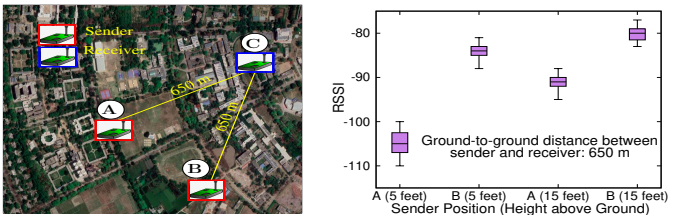

(a) Deployment scenario (b) Signal strength

Fig. 1: The signal strength for different locations.

that signal strength from A is weaker than from B at 5 feet height due to more obstructions between A and C. At 15 feet height, the signal strength at A significantly improves compared to the increase observed at B, attributed to smaller buildings no longer obstructing the signal. This highlights the impact of transceiver height and environmental blockages on LoRa link quality, prompting the development of a more accurate propagation loss model. This work is driven by the following motivations:

Gateway connectivity assurance: The reliable reception of packets in LoRaWAN communication depends upon the RSSI. Estimating accurate RSSI ensures the necessary conditions for reaching a gateway. This aids network operators in deployment planning.

Gateway placement optimization: Accurate RSSI estimation assists in identifying the most suitable locations for gateway placement within the network. This ensures effective coverage and reduces the need for costly post-deployment adjustments.

Identify unreachable locations: Understanding the expected

RSSI values at various points within the network can help identify areas with insufficient coverage.
Optimizing mobility: RSSI estimation for mobile nodes is crucial to the changing signal strengths. It optimizes handovers for seamless connectivity during mobility scenarios.
Battery life preservation: Mobile nodes can conserve battery life by adjusting SF and TxPower based on estimated RSSI. This extends the operational lifetime of these nodes.

C. Preliminaries

This section gives an overview of the various path loss models considered in this paper.
• **Ericsson model for free space and terrain loss:** The Ericsson model estimates signal strength for high-frequency mobile communication systems, including LoRa frequencies [11], [12]. Combining free space and terrain loss, it considers factors like distance d between sender and receiver, transmission frequency f, and antenna height of the sender h_s and the receiver h_r. The path loss is given as

$$P_e = a_0 + a_1 \log_{10}(d) + a_2 \log_{10}(h_s) + a_3 \log_{10}(h_s) \times \log_{10}(d) - 3.2 \log_{10}(11.75 h_r)^2 + g(f), \quad (1)$$

where $a_0 - a_3$ constants depend on propagation environment and $g(f)$ is the frequency correction factor.
• **Multiwall-and-floor model for obstruction loss:** This model treats walls and floors as screens, reducing the radio signal strength passing through them [13], [14]. Let P_{d_0} be the path loss at a reference distance d_0, n is the path loss exponent, and d is the distance between the sender and the receiver. Additionally, j and k are the numbers of wall and floor types, respectively, N_{wi} and N_{fi} are the numbers of walls and floors of type i, respectively, and L_{wi} and L_{fi} are the penetration loss for the wall and floor of type i, respectively. Then, the obstruction path loss is given as

$$P_o = P_{d_0} + 10n \log_{10}\left(\frac{d}{d_0}\right) + \sum_{i=1}^{j} N_{wi} L_{wi} + \sum_{i=1}^{k} N_{fi} L_{fi}. \quad (2)$$

• **First Fresnel Zone (FFZ) in LoRa:** It is a 3D ellipsoid-shaped region around direct path of a radio signal [3]. In LoRa signal propagation, obstacles within FFZ can cast shadows. A point Q lies on the surface of the FFZ if $\sqrt{d_1^2 + r^2} + \sqrt{d_2^2 + r^2} = (d_1 + d_2) + \lambda/2$, where λ represents the wavelength and r denotes the radius of FFZ at point Q. Point Q is situated d_1 away from the sender and d_2 away from the receiver. This condition defines confocal prolate ellipsoidal-shaped regions with the sender and receiver at focal points. The FFZ size increases with signal wavelength, making LoRa's FFZ relatively large due to its low frequency. This emphasizes the importance of considering shadowing in LoRa, beyond the direct path.

III. Study of LoRaWAN in Deployment Scenarios

This paper considers a campus site with distinct characteristics that can significantly impact LoRa signal propagation. The aim is to build a path loss model that realistically represents the campus site by focusing on the following aspects:
Building Diversity: A typical campus includes a variety of buildings, including academic, residential, and administrative structures. Each building impacts signal propagation distinctly due to its varied dimensions.
Open spaces: Large open areas like fields, squares, and courtyards are integral to the campus layout. These spaces often allow for clearer signal paths compared to more densely built-up areas. Besides open spaces, it's vital to address scenarios where a path is unblocked but nearby structures introduce obstructions. These can cause localized shadowing or reflections, impacting signal propagation within the campus.
Foliage and greenery: The presence of trees and landscaped areas introduce natural elements into the signal path, significantly impacting signal, especially at higher frequencies [3].

To accurately design a path loss model for LoRa, it is crucial to understand how the signal propagates. We conducted preliminary experiments to investigate LoRa signal characteristics within a campus site and conclusions are as follows:

1) Line of sight path signal strength: The experiment aims to evaluate the impact of Line of Sight (LoS) on LoRa signal strength by comparing two scenarios: (A to B) and (C to D), as shown in Fig. 2(a). In both scenarios, the distance between the sender and receiver remained constant, and all nodes were positioned at a height of 10 feet. Notably, both LoS paths are unobstructed, but in scenario (A to B), the path is devoid of nearby structures, while in scenario (C to D), the path is in proximity to buildings without direct LoS obstruction. As shown in Fig. 2(b), the received signal at B is stronger than at D, attributed to the shadowing effect from a nearby building in the second scenario.
Observation: *These findings emphasize the importance of considering not only the obstructions in LoS but also the potential impact of nearby structures on signal strength.*

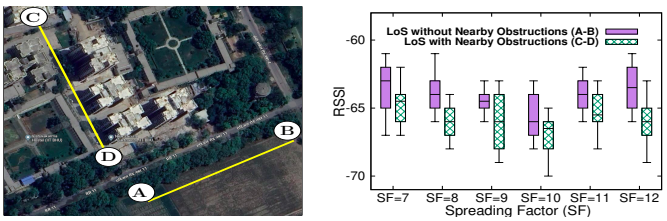

(a) LoS settings (b) Signal strength

Fig. 2: Comparisons between different LoS settings.

2) Non line of sight path signal strength: This study evaluates the impact of Non-Line of Sight (NLoS) conditions on LoRa signal path loss. A receiver is fixed at 5 feet, while the sender's height varies from 5 to 35 feet, as shown in Fig. 3(a). Fig. 3(b) highlights distinct observations in both LoS and NLoS scenarios. Signal strength in LoS slightly decreases with higher sender height, mainly due to the elevated position lengthening the LoS distance. In the NLoS scenario, with the sender and receiver on opposite sides of a building, signal strength significantly decreases as sender height increases. This increase causes the signal to intersect more floors, substantially increasing path loss.
Observation: *These findings underscore the importance of considering the influence of intersected floors and walls in path loss calculations, especially in NLoS scenarios.*

3) Mobile node signal strength: This study aims to investigate the impact of mobility of nodes on LoRa signal strength by conducting experiments with a fixed receiver height of 30 feet. A sender, attached to a bike, traversed along a predetermined path around the receiver, as shown in Fig. 4(a).

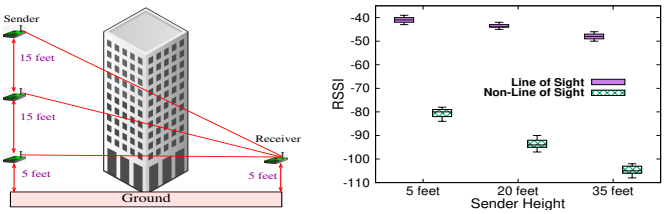

(a) NLoS settings (b) Signal strength

Fig. 3: Comparison between different NLoS settings.

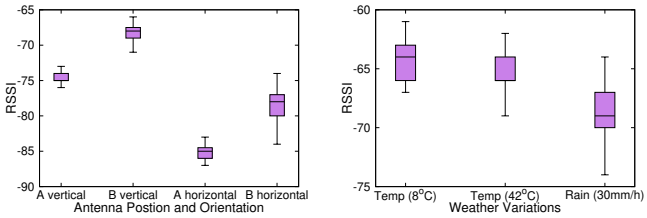

(a) Antenna variation (b) Weather conditions

Fig. 5: RSSI under antenna variation and weather conditions.

The sender maintained SF = 10, TxPower = 18dBm, and transmitted packets at 10ms intervals. Sender speeds varied at 20, 40, and 60 kilometers per hour (kmph). The results, presented in Fig. 4(b), reveal a notable decrease in signal strength with higher sender speeds. This decline was attributed to the increasing effects of Doppler shift and fading.

Observation: *These findings emphasize the importance of considering mobility-related factors when assessing and optimizing LoRa signal performance in dynamic environments.*

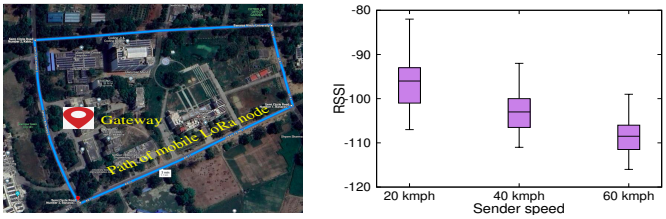

(a) Mobile node path (b) Signal strength

Fig. 4: The signal strength under varying sender speed.

4) Impact of antenna orientation: For this analysis, the receiver is fixed at a height of 30 feet with its antenna oriented vertically at 90 degrees. Two senders, A and B, are positioned at a height of 2 feet and 20 feet, respectively. Both sender antennas are oriented at 180 degrees in both vertical and horizontal positions, resulting in four distinct measurement combinations, as shown in Fig. 5(a). Results indicate B consistently exhibited stronger signals than A due to its higher position offering a clearer path to the receiver. Moreover, vertical antenna orientation at the sender yields better signal strength than horizontal positioning.

Observation: *The findings underscore the importance of considering both sender height and antenna orientation in optimizing LoRa signal strength.*

5) Weather impact on signal strength: The analysis of different weather conditions on LoRa signal strength reveals distinctive impacts. Experiments are conducted across varied climates: a low temperature of 8 degrees Celsius, a high temperature of 42 degrees Celsius, and during heavy rainfall at 30 mm/h. The results depicted in Fig. 5(b) show a slight decrease in signal strength at high temperatures compared to low temperatures. Conversely, heavy rainfall led to a notable decrease in signal strength.

Observation: *This finding emphasizes the significance of considering weather conditions' impact, particularly precipitation, on signal strength.*

IV. Design of MPLoRa

This section introduces a solution for selecting site-specific **LoRa**WAN parameters using **M**ulti-loss **P**ropagation model, abbreviated as MPLoRa. Initially, it identifies obstructions in the communication path between the sender and receiver. Subsequently, a multi-loss propagation model for LoRa signals is developed, incorporating a dynamic adaptation mechanism. Finally, it determines the optimal LoRaWAN parameters.

A. Finding obstructions between sender and receiver

In a typical campus site, buildings and vegetation can obstruct the direct communication path between the sender and receiver. To check for obstructions, we determine the height of structures like buildings and vegetation in the path. If obstruction is present, we then estimate the number of walls and floors affecting the LoS between the sender and receiver.

1) Estimation of the height of obstruction: We utilize Google Earth satellite images to estimate obstruction height, which often lacks complete structural information. We have developed a universally applicable comprehensive method. It begins with image acquisition and advances through shadow detection, image preprocessing, obstruction segmentation, and finally leading to height estimation, as shown in Fig. 6.

• **Capturing satellite image:** The objective here is to acquire a high-resolution RGB satellite image covering the FFZ area between a LoRa sender and receiver to find the obstruction in the communication path. Utilizing specified GPS coordinates, we leverage the $leafmap$ Python library for image retrieval, shown in Fig. 6(a). To enhance image quality and processing efficiency, we partition the covered area into smaller segments.

• **Shadow detection:** After obtaining satellite images, shadows are identified utilizing the method detailed in [15]. These shadows, distinguished by reduced brightness, are detected through an analysis of luminance levels in the RGB image. It is then transformed into YCbCr color space using the $cv2$ (OpenCV) library, where 'Y' represents luminance whereas 'Cb' and 'Cr' denote chromaticity. Subsequently, a binary shadow mask is generated based on luminance mean, standard deviation, and an adjustable threshold, as depicted in Fig. 6(b). The resultant shadow mask image is saved as I_{mask}.

• **Preprocessing of the satellite image:** After shadow detection, the satellite image undergoes preprocessing to enhance the clarity of structures. Using the previously generated shadow mask, we counterbalance the shadow effects. This process highlights the buildings and lays the foundation for effective segmentation as shown in Fig. 6(c).

• **Obstruction segmentation:** The segmentation in the preprocessed satellite image, isolates entities for detailed analysis, focusing on building and vegetation structures. We use SamGeo library [16] for image segmentation. For vegetation segmentation, the sam.predict() function with a 'tree' prompt is used to detect and visualize vegetation areas as in Fig. 6(d), saved as segmented vegetation images (I^v_{seg}). Similarly, a 'building' prompt aids in identifying and visualizing building

footprints in the satellite image, depicted in Fig. 6(e), resulting in segmented building images (I^b_{seg}). We then proceed to height estimation from the segmented images.

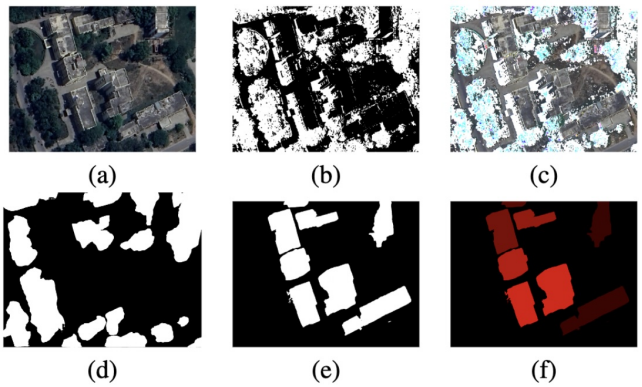

Fig. 6: Estimation of height of the obstructions. Parts (a)-(f) illustrate satellite image, shadow mask, preprocessed image, vegetation segmentation, building segmentation, and building heights images.

• **Obstruction height estimation:** The final step involves estimating the height of the obstruction. In the case of vegetation, we take the average height of vegetation across the campus. Building heights are determined using the approach given in [17]. Each segmented building is analyzed in conjunction with its shadow from the mask. The length of the shadow, combined with the provided solar azimuthal and solar elevation angles provide insights into building height based on trigonometric principles. Once the heights of all buildings are computed, this data is encoded and saved in the .tif image format. This image functions as a height map, with each pixel value representing the building's height at that specific location. To provide a clearer understanding, we create an RGB image where building heights are visually conveyed on a red scale as shown in Fig. 6(f), with deeper shades of red indicating greater height. The steps of obstruction height estimation are given in Procedure 1. After estimating the height, we ascertain whether it obstructs the communication path. If so, we proceed to identify the number of walls and floors obstructing the path in the case of the building.

2) Estimation of number of walls and floors: To estimate the number of walls and floors a signal traverses within a building, we assume uniform floor heights and consistent wall spacing. Fig. 7 provides a visual representation of how we calculate the number of walls and floors intersected by the signal. Let x and y represent the uniform distances between consecutive walls and floors, respectively. Considering d as the ground-to-ground distance between the sender and receiver, and h_s and h_r denoting their respective heights, $\theta = \arctan\left(\frac{|h_s - h_r|}{d}\right)$ represents the angle between LoS link and horizontal line through the building. The horizontal straight-line distance through the building that the signal traverses, denoted as d', is directly used to calculate the number of walls (N_w) and floors (N_f). The vertical height difference between the entry and exit points of the signal in the building is given by $d' \tan\theta$. The numbers of walls and floors are therefore calculated as

$$N_w = \left\lceil \frac{d'}{x} \right\rceil \text{ and } N_f = \left\lceil \frac{d' \times \tan\theta}{y} \right\rceil. \quad (3)$$

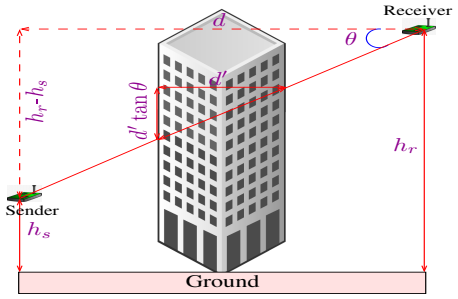

Fig. 7: Estimation of walls and floors.

Procedure 1: Obstruction height estimation

Input: Shadow mask image (I_{mask}), building and vegetation segmented image (I^b_{seg}, I^v_{seg}), solar azimuthal angle (θ_a), solar elevation angle (θ_e)
Output: Height estimated image (I_h)
Initialization: $I_h = np.zeros\_like(I_{mask})$, $H_r = []$;
Preprocess I_{mask}, I^v_{seg}, and I^b_{seg} by obtaining dimensions and applying padding to the mask;
Find shadow bearing and polar angle (θ_p) using θ_a and θ_e;
for *each vegetation region* (V_r) *in* I^v_{seg} **do**
    Trace boundary of V_r;
    Assign average vegetation height to all pixels in V_r region in I_h;
for *each building region* (B_r) *in* I^b_{seg} **do**
    Trace boundary of B_r;
    for *height* (h_{test}) *in a range of possible building heights* **do**
        Calculate shadow length $L = \frac{h_{test}}{\tan(\theta_p)}$;
        Obtain shadow length L' from I_{mask} corresponding to B_r region;
        Compute Jaccard similarity score $J(L, L')$;
        Append h_{test} and corresponding $J(L, L')$ to H_r;
    Optimal height (h_{opt}) $= \max(H_r)$;
    Assign h_{opt} to all pixels in B_r region in I_h;
Save I_h with computed obstruction heights;
return I_h;

B. Formulation of the multi-loss propagation model

We integrate the Ericsson model for free space and terrain loss with the Multiwall-and-floor model to address obstruction loss due to walls and floors. These models are selected for their consideration of key path loss factors and their demonstrated effectiveness in our experimental research on LoRa path loss estimation. To further refine the model, we introduce a composite shadow fading term. This term accounts for additional losses arising from obstruction of the FFZ by buildings and foliage. Let N_{build} and N_{fol} denote the counts of points obstructed by buildings and foliage, respectively within the FFZ. To calculate the values of N_{build} and N_{fol}, we partition the FFZ into equally spaced planes following a similar approach to Flog [3]. The number of sampling points on a plane i is determined by the equation $N_{i_{\text{plane}}} = \frac{N_{\text{ref}} \times S_i}{4\pi d_i^2}$, where N_{ref} is an adjustable constant, S_i is the area of the plane, and d_i is the distance from the sender to the plane. This reflects the decrease in sampling points with increasing distance due to the drop in signal energy. At each point, we assess whether it is obstructed by either campus buildings or foliage. The cumulative counts from all planes determine N_{build} and N_{fol}. These counts integrate into the shadow fading term, capturing the impact of physical obstructions by buildings and foliage

within the FFZ. By using Eqs. 1, 2, 3, and FFZ condition, the final path loss is given by

$$P = a_0 + a_1 \log_{10}(d) + \log_{10}(h_s)(a_2 + a_3 \log_{10}(d)) - 6.4\times \log_{10}(h_r) + \sum_{i=1}^{j} N_{wi} L_{wi} + \sum_{i=1}^{k} N_{fi} L_{fi} + X_1 N_{\text{build}} + X_2 N_{\text{fol}}, \tag{4}$$

where X_1 and X_2 are the scaling factors for buildings and foliage, respectively. We determine the distance d between sender and receiver using the Haversine formula [18] as

$$d = 2R \cdot \arcsin\left(\sqrt{\alpha}\right), \tag{5}$$

where $\alpha = \sin^2\left(\frac{\Delta\phi}{2}\right) + \cos(\phi_s)\cos(\phi_r)\sin^2\left(\frac{\Delta\lambda}{2}\right)$, ϕ_s and ϕ_r are respectively the latitudes of the sender and receiver in radians, $\Delta\phi$ and $\Delta\lambda$ denote the differences in latitude and longitude between the sender and receiver in radians, respectively, and R is the radius of the Earth. To accurately determine the values of $a_0 - a_3, X_1$, and X_2, a linear regression algorithm is employed, analyzing data collected from a single sender-receiver pair. Diverse signal propagation scenarios are captured, incorporating variations in sender-receiver height, distance, and obstructions within the FFZ. The linear regression model is trained to identify optimal parameter values, reflecting the impact of distance, obstruction, and height variations on path loss. Our analysis yielded optimal values for the parameters: $a_0 = 37.4$, $a_1 = 30.2$, $a_2 = -14.3$, $a_3 = 0.08$, $X_1 = 0.07$, and $X_2 = 0.02$.

C. Dynamicity adaptation mechanism

The variables of the multi-loss propagation model are subject to change based on dynamic environmental factors on the campus, encompassing the following range of situations:

- *Mobility of transceivers*: Observations indicate that path loss increases with the speed of the mobile transceiver.
- *Campus infrastructure changes:* Long-term alterations in the campus layout, including new constructions or removal of existing structures, can significantly impact the signal strength.
- *Variation in weather seasons:* Changes in weather conditions such as temperature and precipitation can affect the propagation of signals.

To incorporate mobility, we introduce a speed-dependent factor $f(v)$ into Eq. 4, where v denotes the speed of the mobile transceiver. By collecting data from mobile transceivers operating at different speeds, we calculate an average path loss specific to speed ranges. This information is instrumental in calibrating the speed-dependent factor. To accommodate changes in campus infrastructure, it is imperative to regularly update the campus map and structural data in the database, ensuring alignment with the latest developments. As for variations in weather seasons, we employ a method similar to Flog to adapt to these changes. Leveraging recent RSSI data from nodes and focusing on the last 10 packets, our model effectively incorporates real-time weather conditions. Recalibrating the variables $a_0 - a_3, X_1$, and X_2 is achieved through a non-linear least squares fitting algorithm [19]. This ensures the ongoing adaptation of our model to signal changes caused by varying weather conditions.

D. Network parameter optimization

This section presents a methodology for optimizing LoRaWAN parameters (SF and TxPower) using the estimated path loss from our proposed multi-loss propagation model. By using the obtained path loss from Eq. 4, the minimum achievable RSSI for the sender ($RSSI_{min}$) is given as

$$RSSI_{min} = TxP_{min} + g_s + g_r - P, \tag{6}$$

where g_s and g_r are the antenna gains for sender and receiver, respectively, and TxP_{min} is the senders' minimum TxPower. Procedure 2 outlines the steps for determining the optimal SF SF_{opt} and TxPower TxP_{opt}. The procedure begins by computing the minimum achievable RSSI ($RSSI_{min}$) for the sender using Eq. 6. Subsequently, $RSSI_{min}$ is compared to the receiver sensitivity at the minimum SF ($RxS_{SF_{min}}$). If the combination of $RxS_{SF_{min}}$ and an RSSI margin value ($RSSI_{margin}$) is not greater than $RSSI_{min}$, then the minimum SF (SF_{min}) and minimum TxPower (TxP_{min}) are considered as the optimal SF and optimal TxPower, respectively. However, if the required signal strength is not met, the procedure checks whether increasing the TxPower can achieve the desired signal strength. If, even after maximizing TxPower (TxP_{max}), the required signal strength is not attained, the SF is incremented by one, and TxPower is recalculated based on the new receiver sensitivity. This iterative process continues until the desired signal strength is achieved. Ultimately, the optimal SF and TxPower are determined as the minimum SF and TxPower required to attain the desired signal strength.

Procedure 2: Optimal SF and TxPower estimation for the sender

Input: Sender and receiver antenna gain (g_s, g_r), $SF_{min/max}$, $TxP_{min/max}$, $RSSI_{margin}$;
Output: SF_{opt} and TxP_{opt};
Estimate $RSSI_{min}$ using Eq. 6;
if $RSSI_{min} \geq (RxS_{SF_{min}} + RSSI_{margin})$ **then**
  $SF_{opt} = SF_{min}$;
  $TxP_{opt} = TxP_{min}$;
else
  $SF_{req} = SF_{min}$;
  $TxP_{req} = TxP_{min} + RxS_{SF_{min}} - RSSI_{min} + RSSI_{margin}$;
  while *($TxP_{req} > TxP_{max}$ **AND** $SF_{req} < SF_{max}$)* **do**
    $SF_{req} = SF_{req} + 1$;
    $TxP_{req} = TxP_{min} + RxS_{SF_{req}} - RSSI_{min} + RSSI_{margin}$;
  $TxP_{opt} = \min(TxP_{req}, TxP_{max})$;
  $SF_{opt} = SF_{req}$;
return SF_{opt}, TxP_{opt};

Algorithm 1 illustrates all the steps of MPLoRa, which include Procedure 1 and Procedure 2 for selecting site-specific LoRaWAN parameters using the Multi-loss Propagation model. By employing Algorithm 1, the MPLoRa can effectively estimate optimal SF and TxPower settings, ensuring reliable and efficient communication between the sender and receiver.

V. Performance Evaluation

To evaluate the proposed MPLoRa, we integrate Optimal Data Rate (ODR) and Terrain Analysis (TA) handlers into the Network Server (NS). The ODR handler incorporates

Algorithm 1: MPLoRa

Input: Deployment site layout, GPS coordinates $(\phi_s, \phi_r, \Delta\lambda)$;
Output: LoRaWAN parameters, obstructions in site;
Obtain FFZ satellite images of the site using GPS coordinate values of sender and receiver;
Calculate distance d between sender and receiver by Eq. 5;
Estimate obstructions height using satellite images as given in Procedure 1;
if *(height obstructs LoS communication path)* **then**
  if *(obstruction is building)* **then**
    Estimate the number of walls N_w and floors N_f intersecting using Eq. 3;
  else
    Assign $N_w = N_f = 0$;
Calculate the counts of points in FFZ obstructed by buildings, N_{build}, and by foliage, N_{fol};
Obtain path loss $P(d, N_w, N_f, N_{\text{build}}, N_{\text{fol}})$ from Eq. 4;
Modify Eq. 4 to adapt change in the environment using dynamicity adaption mechanism;
Determine the SF_{opt} and TxP_{opt} using Procedure 2;
return SF_{opt},TxP_{opt}, receiving power, obstructions in site

the proposed multi-loss propagation model and determines optimal SF and TxPower for the sender based on height and location relative to the receiver. The TA handler is responsible for computing essential environmental features, including the number of walls, floors, and obstructions height. ODR module uses this information to determine the optimal SF and TxPower configuration for each sender. To communicate the new SF and TxPower settings to the nodes, the NS utilizes the LinkADRReq MAC command. For the implementation, chirpstack LoRaWAN server stack [20] is utilized along with The Things Outdoor gateway (868MHz) and commercial off-the-shelf LoRaWAN nodes. We evaluate the performance of MPLoRa considering deployment region and mobility and compare it with baseline models. The dataset and code for our evaluation are available in [9].

A. Impact of deployment region

We assess the proposed multi-loss propagation model against four LoRa baseline models: Okumura Hata Model [21], Log Distance Model [22], and Lebanon Campus Model [23]. Okumura Hata considers distance, frequency, and antenna heights, addressing urban effects but does not consider obstruction. Log Distance incorporates flat fading but lacks antenna height and obstruction considerations. Lebanon Campus includes campus-specific antenna height effects but neglects obstruction and diffraction. The evaluation utilizes our collected signal strength dataset, and we employ the absolute error metric, calculated as $|y_i - \hat{y}_i|$, where y_i and $\hat{y}_i$ are the actual and estimated RSSI value of the i-th packet, respectively. Table I presents the average estimation errors and standard deviations of the pathloss models in LoS and NLoS scenarios. The proposed model significantly outperforms the baseline models in both scenarios.

• **Impact on LoS communication:** Fig. 8(a) to Fig. 8(d) depict the evaluation results for the LoS scenario. Specifically, Fig. 8(a) and Fig. 8(c) show the absolute RSSI error for the path loss models at different distances and heights, respectively, highlighting the superior accuracy and consistency of our model over baseline models. The stability in absolute error underscores the robustness of our design, attributed to

TABLE I: Absolute RSSI Estimation Errors in LoS and NLoS Scenarios.

Approach	LoS Scenario		NLoS Scenario	
	Avg.	Std. Dev.	Avg.	Std. Dev.
Okumura Hata	6.64	3.91	15.85	6.44
Log Distance	6.11	4.01	15.55	7.89
Lebanon Campus	7.17	3.86	13.02	6.36
Proposed Model	2.46	1.55	4.38	2.75

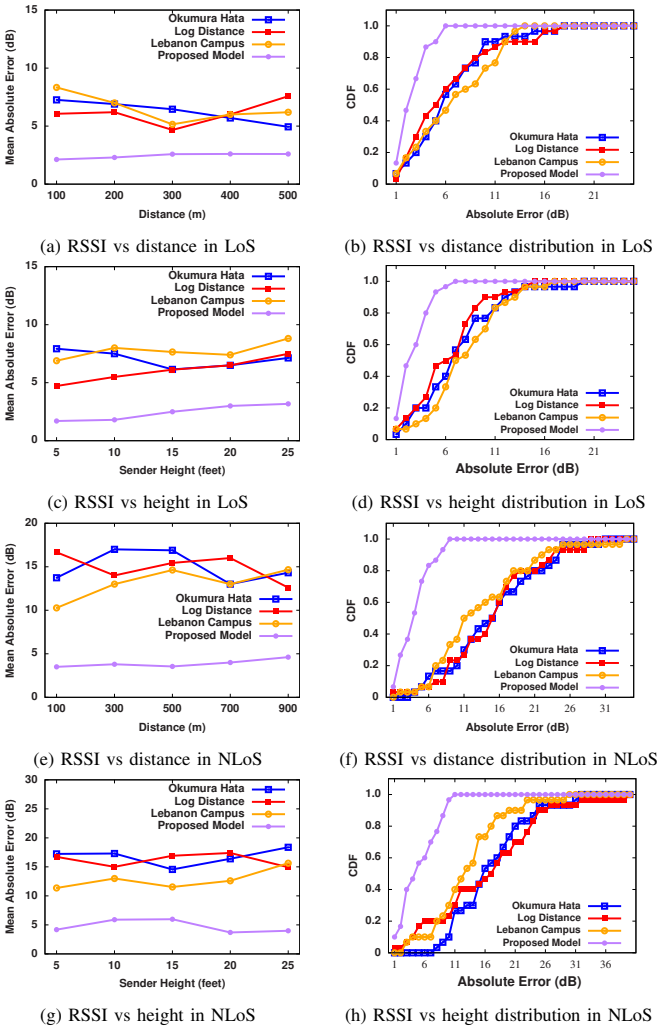

(a) RSSI vs distance in LoS
(b) RSSI vs distance distribution in LoS
(c) RSSI vs height in LoS
(d) RSSI vs height distribution in LoS
(e) RSSI vs distance in NLoS
(f) RSSI vs distance distribution in NLoS
(g) RSSI vs height in NLoS
(h) RSSI vs height distribution in NLoS

Fig. 8: Comparison with existing models in LoS and NLoS scenario.

comprehensive features and FFZ obstruction consideration. Fig.8(b) and Fig.8(d) further provide insights into the Cumulative Distribution Function (CDF) of absolute RSSI errors. Fig.8(b) indicates that, in distance-based evaluations, the CDF reaches 1 at an absolute RSSI error of 6, signifying that all errors fall within this range. In contrast, Fig.8(d) reveals a CDF of 0.97 for the same error in height measurements, emphasizing how distance and height distinctly influence the LoS signal error distribution.

• **Impact on NLoS communication:** Fig. 8(e) and Fig. 8(g) depict the evaluation results for the NLoS scenario under varying distances and heights, respectively. As in the case of the LoS scenario, the proposed model shows better performance compared to all the baseline models. It performs reliably despite the challenges inherent in NLoS environments where obstructions such as buildings and foliages introduce greater errors and variability. Fig. 8(f) and Fig. 8(h) depict the CDF of absolute RSSI error for distance and height evaluations, respectively. The distance-based CDF value reaches 1.0 at an

RSSI error of 9, while the height-based evaluation registers a CDF of 0.95 at the same error level, showing a significant performance improvement over baseline models.

Observation: *The main highlight is that increasing distance leads to errors in both LoS and NLoS due to more free space loss in LoS and potential obstructions in NLoS. Conversely, height increase amplifies LoS errors by elongating the path but reduces NLoS errors by mitigating obstructions.*

B. Impact of mobility

We validate the proposed approach on mobile devices, distinguishing between unconfirmed and confirmed messages. The evaluation covers key network performance metrics, such as Packet Reception Ratio (PRR), Packet Delivery Time (PDT), energy consumption, and throughput.

Evaluation setup: For this evaluation, we use the transceiver, Chirpstack server, and Things outdoor gateway. We established the gateway at a height of 30 feet while maintaining the node at a height of 5 feet. To reduce the complexity, the deployment region is divided into grids as shown in Fig. 9(a). Fig. 9(b) and Fig. 9(c) show the distribution of SF and TxPower across grids, respectively. Notably, the equidistant regions or grids around the gateway exhibit varying optimal SF and TxPower values. This variation could be attributed to the heterogeneous nature of the environment, where different levels of obstructions impact signal propagation differently. The LoRa node is attached to a mobile vehicle that moves through a fixed path at the speed of 10kmph within the deployment region, as shown in Fig. 9(a). To evaluate our approach, we compare it against two fixed approaches with SF set to 7 and 12.

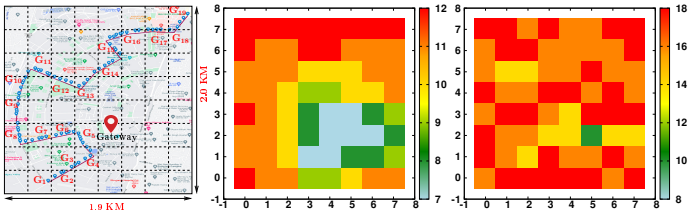

(a) Path profile (b) SF distribution (c) TxPower distribution

Fig. 9: The path profile of the mobile LoRa node and distribution of SF and TxPower across grids.

• **Impact on unconfirmed messages:** We evaluate the performance of the proposed approach on unconfirmed messages. Fig.11(a) shows the PRR of the considered approaches across various grids. The proposed approach consistently outperforms SF = 7 and performs comparably to SF = 12 in terms of PRR. In Fig.10(a) to Fig. 10(d), we present energy consumption, throughput, effective throughput, and PDT respectively, across grids. Effective throughput is defined as the product of raw throughput and PRR. The proposed approach outperforms SF = 12 approach in all aspects. These improvements are attributed to the proposed approach's optimal selection of SF and TxPower settings for different grid settings that were either lower or equal to those of the SF = 12 approach. Employing optimal settings enables the proposed approach to achieve high PRR, reduced energy consumption, improved effective throughput, and faster packet delivery.

• **Impact on confirmed messages:** In this assessment, we set the maximum allowed retransmissions to 3. Similar to

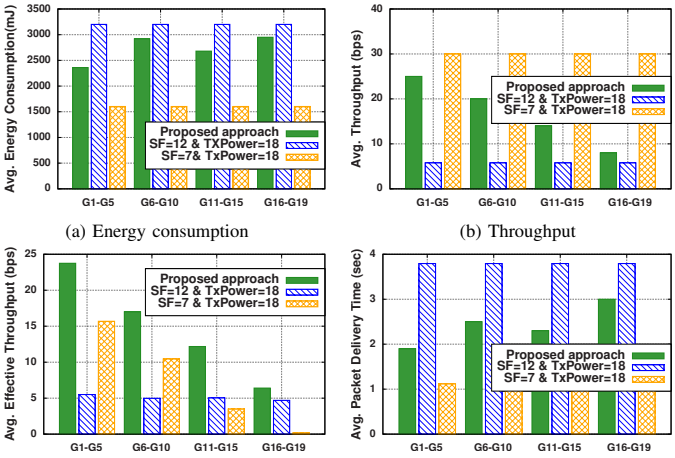

(a) Energy consumption (b) Throughput

(c) Effective throughput (d) Packet delivery time

Fig. 10: Impact of mobility on unconfirmed messages.

the results of unconfirmed messages, our proposed approach surpasses SF = 7 and performs comparably to SF = 12 in terms of PRR as in Fig.11(b). Regarding the number of retransmissions required to deliver a packet successfully, both our approach and SF = 12 outperform SF = 7 as shown in Fig.12(a). However, when it came to energy consumption, effective throughput, and PDT, the proposed approach stood out significantly better than the other approaches, as shown in Fig. 12(b) to Fig. 12(d), respectively. For confirmed messages, we define the "effective throughput" as the rate considering only the size of a single packet (excluding retransmissions) over the total time until acknowledgment. These findings underscore the substantial advantages of our approach, rendering it more efficient and faster in handling confirmed messages compared to alternative approaches.

Observation: *An interesting observation from the result is that the fixed approach at SF = 7 conserves energy and PDT but fails to reach the receiver when the distance is greater, while the fixed approach at SF = 12 successfully transmits the packet but consumes significant energy and time.*

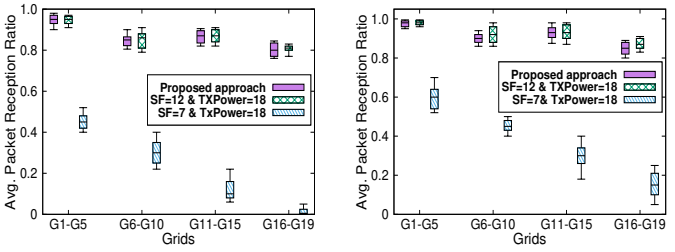

(a) Unconfirmed (b) Confirmed

Fig. 11: Comparison for unconfirmed and confirmed messages.

C. Comparison with existing work

Finally, we compare the MPLoRa with the existing approaches, including ESSS [24], CALR [1], and OptSF [4]. We present comparative results in terms of relative absolute error and PRR. Figure 13(a) shows the error difference between the existing model (Okumura) and the proposed multi-loss propagation model. As the distance between sender and receiver increases, the relative error of the approaches also increases. This is because the increase in distance increases the number of obstructions in a communication path, which

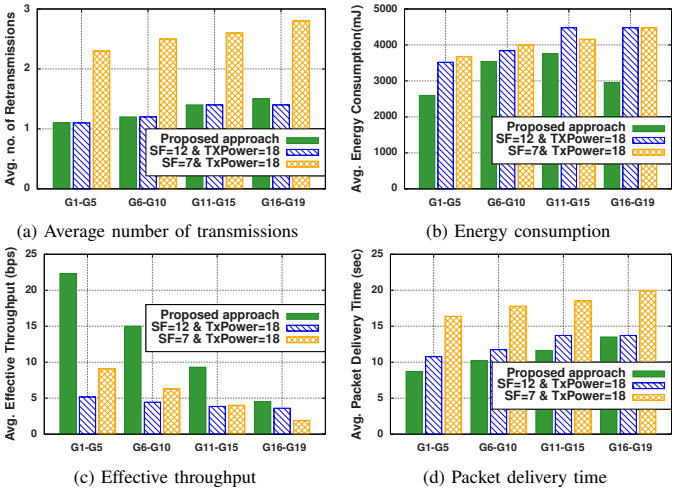

(a) Average number of transmissions (b) Energy consumption

(c) Effective throughput (d) Packet delivery time

Fig. 12: Impact of mobility on confirmed messages.

results in a higher value of relative error. Further, we can make a similar observation for relative PRR as shown in Fig. 13(b).

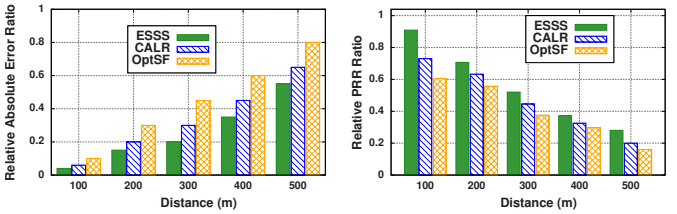

(a) Absolute error (b) PRR

Fig. 13: Comparison with the existing work.

VI. Conclusion

This paper analyzed LoRa signal propagation across diverse scenarios, highlighting that deployment site scenarios and the positions of the sender and receiver influence the communication range in LoRaWAN. The constrained range is attributed to signal absorption and reflection by obstructions such as buildings, vegetation, and the ground. The paper proposed a solution for selecting site-specific LoRaWAN parameters using a multi-loss propagation model. It introduces automated obstruction detection in unknown sites, eliminating the need for manual intervention. Considering the detected obstructions, it estimates path loss, which helps to determine the optimal network parameter settings in LoRaWAN. Experimental results confirmed the effectiveness of the proposed work, showcasing improvements in communication efficiency and overall network performance. This contribution underscores the potential of the work to enhance LoRaWAN deployments across diverse and challenging environments.

The future research direction of this work involves expanding the solution to include multi-hop LoRaWAN deployment, enhancing scalability for wider communication. Additionally, it is imperative to generalize the learned models and algorithms to effectively adapt to diverse environmental conditions and deployment setups.

Acknowledgment

This work was supported by I-DAPT HUB FOUNDATION, IIT (BHU) Varanasi under grant RD/SA/I-DAPT IIT (BHU)/CSE/23-24/02/494 and SERB under grant MTR/2023/000764.

References

[1] P. Kumari, H. P. Gupta, T. Dutta, and S. K. Das, "Improving Age of Information with Interference Problem in Long-Range Wide Area Networks," in *Proc. IEEE WoWMoM*, 2022, pp. 137–146.

[2] L. Liu, Y. Yao, Z. Cao, and M. Zhang, "DeepLoRa: Learning Accurate Path Loss Model for Long Distance Links in LPWAN," in *Proc. IEEE INFOCOM*, 2021, pp. 1–10.

[3] K. Yang, Y. Chen, X. Chen, and W. Du, "Link Quality Modeling for LoRa Networks in Orchards," in *Proc. ACM IPSN*, 2023, p. 27–39.

[4] J. C. Liando, A. Gamage, A. W. Tengourtius, and M. Li, "Known and unknown facts of lora: Experiences from a large-scale measurement study," *ACM Trans. Sen. Netw.*, vol. 15, no. 2, feb 2019.

[5] M. Slabicki, G. Premsankar, and M. Di Francesco, "Adaptive configuration of lora networks for dense IoT deployments," in *Proc. IEEE IFIP NOMS*, 2018, pp. 1–9.

[6] R. E. Navas, G. Dandachi, Y. Hadjadj-Aoul, and P. Maillé, "Energy-Aware Spreading Factor Selection in LoRaWAN Using Delayed-Feedback Bandits," in *Proc. IEEE IFIP*, 2023, pp. 1–9.

[7] "Understanding adr — developer portal," 2024. [Online]. Available: https://lora-developers.semtech.com/documentation/tech-papers-and-guides/understanding-adr/

[8] L. Amichi, M. Kaneko, E. H. Fukuda, N. El Rachkidy, and A. Guitton, "Joint Allocation Strategies of Power and Spreading Factors With Imperfect Orthogonality in LoRa Networks," *IEEE Trans. on Communications*, vol. 68, no. 6, pp. 3750–3765, 2020.

[9] "MPLoRa." [Online]. Available: https://sites.google.com/view/lorawanifip/home

[10] Z. Qin and J. A. McCann, "Resource efficiency in low-power wide-area networks for iot applications," in *GLOBECOM 2017 - 2017 IEEE Global Communications Conference*, 2017, pp. 1–7.

[11] M. A. E. S. A. El Nashar and M. Sherif, *Design Deployment and Performance of 4G-LTE Networks: A Practical Approach*. U.K.:Wiley, 2014.

[12] M. Stusek, D. Moltchanov, P. Masek, K. Mikhaylov, O. Zeman, M. Roubicek, Y. Koucheryavy, and J. Hosek, "Accuracy Assessment and Cross-Validation of LPWAN Propagation Models in Urban Scenarios," *IEEE Access*, vol. 8, pp. 154 625–154 636, 2020.

[13] A. Ben Zineb and A. Mohamed, "A Multi-wall and Multi-frequency Indoor Path Loss Prediction Model Using Artificial Neural Networks," *Arabian Journal for Science and Engineering*, vol. 41, 11 2015.

[14] M. Lott and I. Forkel, "A multi-wall-and-floor model for indoor radio propagation," in *Proc. IEEE VTS*, vol. 1, 2001, pp. 464–468 vol.1.

[15] K. Deb and A. H. Suny, "Shadow Detection and Removal Based on YCbCr Color Space," *Smart Comput. Rev.*, vol. 4, pp. 23–33, 2014. [Online]. Available: https://api.semanticscholar.org/CorpusID:16038715

[16] "Segment anything," https://segment-anything.com/, accessed: 2024-02-14.

[17] N. Kadhim and M. M. Mourshed, "A Shadow-Overlapping Algorithm for Estimating Building Heights From VHR Satellite Images," *IEEE Geoscience and Remote Sensing Letters*, vol. 15, pp. 8–12, 2018. [Online]. Available: https://api.semanticscholar.org/CorpusID:3211746

[18] R. W. Sinnott, "Virtues of the Haversine," *Sky and telescope*, vol. 68, no. 2, p. 158, 1984.

[19] M. Johnson, "Nonlinear Least-Squares Fitting Methods," *Methods in cell biology*, vol. 84, pp. 781–805, 02 2008.

[20] C. open-source LoRaWAN Network Server, 2024. [Online]. Available: https://www.chirpstack.io/

[21] S. Demetri, M. Zúñiga, G. P. Picco, F. Kuipers, L. Bruzzone, and T. Telkamp, "Automated Estimation of Link Quality for LoRa: A Remote Sensing Approach," in *Proc. IEEE IPSN*, 2019, pp. 145–156.

[22] M. C. Bor, U. Roedig, T. Voigt, and J. M. Alonso, "Do LoRa Low-Power Wide-Area Networks Scale?" in *Proc. ACM MSWiM*, 2016, p. 59–67.

[23] R. El Chall, S. Lahoud, and M. El Helou, "LoRaWAN Network: Radio Propagation Models and Performance Evaluation in Various Environments in Lebanon," *IEEE Internet of Things Journal*, vol. 6, no. 2, pp. 2366–2378, 2019.

[24] P. Kumari, H. P. Gupta, R. Mishra, and S. K. Das, "An Energy-Efficient Smart Space System Using LoRa Network with Deadline and Security Constraints," in *Proc. ACM MSWiM*, 2021, p. 79–86.